FINITE ELEMENT UNIT CELL BASED STRENGTH PREDICTION OF STITCHED CFRP LAMINATES

H. Heß, N. Himmel
Institut für Verbundwerkstoffe (IVW) GmbH,
Erwin-Schrödinger-Straße, Gebäude 58, 67663 Kaiserslautern,
Germany

OVERVIEW

Carbon fiber reinforced plastic laminates (CFRP) show superior stiffness and strength properties relative to their density in comparison to metallic materials, which make them attractive for light-weight applications, namely in the aviation industry. Three-dimensional stress states due to impact loads (bird strike, runway debris) or local load introductions, post special requirements with regard to the mechanical performance of CFRPs, as in most cases no reinforcing fibers are arranged perpendicular to the laminate plane (out-of-plane) to carry corresponding internal stresses. Such effects tend to induce local delaminations in the laminate which may grow during operation and lead to ultimate failure. One method to enhance out-of-plane properties is the stitching of dry semi-finished fiber products in the thickness direction (3D reinforcement) prior to resin infusion. On the other hand, the insertion of a yarn in the thickness direction causes dislocations of the in-plane fibers, which lead to the formation of voids (resin pockets) in the stitch vicinity after resin infusion possibly affecting the in-plane properties of the laminate, such as stiffness and strength.

To quantify the effect of 3D reinforcement in non-crimp fabric (NCF) carbon fiber/epoxy laminates under uniaxial tension loading an experimental study was carried out within LuFo II and III which included a systematic variation of the yarn diameter, the stitching pattern and direction as well as the load direction. Tension test results showed a significant effect of the stitching on the in-plane Young's modulus and strength parallel to the *x* and *y* direction of the laminate which was attributed to local dislocations of the in-plane fibers and changes in the fiber volume fraction.

A finite element (FE) based unit cell model was developed to estimate the in-plane strength properties of 3D stitched NCF carbon fiber laminates. Depending on the aforementioned parameters local changes of the fiber volume fraction as well as regions with undisturbed and disturbed fiber orientations within the laminate layers are taken into account in the model. The non-linear, continuum mechanics based failure analysis includes strain and stress analysis, fracture analysis and degradation analysis. To estimate the stress exposure the maximum stress criterion and Puck's action plane criterion for 3D stress states criterion were applied for fiber and inter-fiber failure, respectively. Post-failure behavior was modeled by partial stiffness degradation according to a Chiu model which was modified for 3D stress states. Applying this failure analysis the strength of stitched and unstitched laminates was predicted for all parameter configurations included in the experimental study and validated against the experimental results.

1. INTRODUCTION

The stitching technology offers the potential for substantial weight and cost reductions in primary structures of passenger airplanes [1]. It eases the subsequent manufacturing process by realizing dry fiber preforms in the demanded geometrical shapes for subsequent resin injection or infusion processes. Moreover, metallic inserts for load introduction elements can be attached to these preforms by stitching. The insertion of 3D reinforcements by stitching provides a possibility to enhance the out-of-plane properties of FRPs ([2], [3]). In comparison to the unstitched laminate the compressive strength after impact can be increased by stitching by more than 80 % [4] and the mode I energy release rate G_{IR} (which may be interpreted as G_{IC} in the case of unstitched laminates) by more than a factor of 4 ([5], [6]).

Adversely, the stitching yarn dislocates the in-plane fibers of the dry preform, which causes resin-rich zones after resin infusion. These voids may affect the in-plane stiffness and strength properties of the laminate. In the manufacturing process of non-crimp fabrics (NCF) stitching with a non-structural binding yarn (FIG. 1 a and b) already disturbs the in-plane fibers creating voids in the composite and inducing an early initiation of damage [7]. Referring to the mechanical properties of structurally stitched FRPs in the laminate plane multiple and contradictory information can be found in the open literature; [8], [9], [10]. Experimental investigations on non-crimp fabric CFRP laminates under in-plane loading which were stitched in the thickness direction of the laminate (FIG. 1 c and d) showed that, depending on the applied stitching parameters, similar Young's moduli resulted at best, but also reduced moduli by up to 29 % compared to the unstitched laminate [11], [12].

2. MATERIALS, MANUFACTURING AND CHARACTERIZATION

2.1. Laminates and stitching parameters

A1, B, and A2 types of carbon fiber non-crimp fabrics manufactured by Saertex GmbH & Co. KG were applied to produce [A1-B-A2] orthotropic laminates with a $[+45/0/-45/0/\overline{90}]_S$ mid-plane symmetric lay-up, as shown in FIG 2. The effect of structural stitching is compared with properties of structurally unstitched laminates where the term "stitched laminates" refers to laminates composed of NCF layers with stitches through the total thickness of the laminate (FIG. 1 c and d). Laminates containing NCFs without structural stitches are denoted as "unstitched laminates".

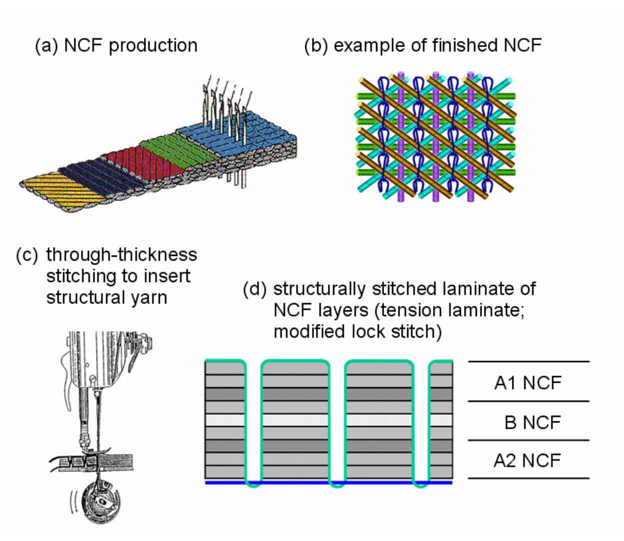

FIG 1. (a, b) NCF manufacturing process, (c, d) structural stitching of [A1-B-A2] NCF lay-up ([12] – [15])

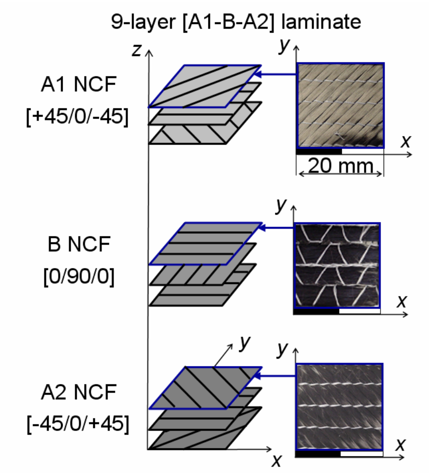

FIG 2. NCF lay-up of [A1-B-A2] CFRP laminate and top views of A1, B and A2 NCFs

In the study the parameters of the structural stitching were varied systematically. 3.3 and 5.0 mm variations of the pitch length *p* (i. e. the distance between two stitches) and the spacing *s* (distance between two parallel seams) in the *x* and *y* direction of the laminate resulted in four stitch patterns with an areal density of 4.00, 6.06 and 9.18 stitches per cm^2. Stitching was carried out with a modified lock stitch (FIG. 1 d) using twisted E-glass stitching yarns with a linear density of 68 tex or 136 tex in the upper and 68 tex in the lower yarn [12]. Together with loading directions parallel to the *x* and *y* axes of the laminates this resulted in a total of $2^5 = 32$ test configurations (TAB 1).

Flat plates with unstitched and structurally stitched NCF lay-ups were impregnated with RTM 6 aerospace grade epoxy resin (Hexcel Composites) in a vacuum assisted resin infusion (VARI) process. In combination with the VARI process, through-thickness stitching influenced the laminate thickness and the fiber volume fraction of the laminate [12] resulting in a maximum increase of the laminate thickness of 7.5 % compared to the unstitched composite and an equivalent reduction of the fiber volume content (yarn diameter 136 tex, stitch density 9.18 1/cm^2). As the alteration of the fiber volume fraction substantially influences the elastic constants of the laminate, this effect needed to be considered in the unit cell model.

parameter configuration	loading direction	stitching direction	linear density of yarn [tex]	spacing s [mm]	pitch length p [mm]
K 1	*x*	*x*	68	5.0	5.0
K 2	*x*	*x*	68	5.0	3.3
K 3	*x*	*x*	68	3.3	5.0
K 4	*x*	*x*	68	3.3	3.3
K 5	*x*	*x*	136	5.0	5.0
K 6	*x*	*x*	136	5.0	3.3
K 7	*x*	*x*	136	3.3	5.0
K 8	*x*	*x*	136	3.3	3.3
K 9	*x*	*y*	68	5.0	5.0
K 10	*x*	*y*	68	5.0	3.3
K 11	*x*	*y*	68	3.3	5.0
K 12	*x*	*y*	68	3.3	3.3
K 13	*x*	*y*	136	5.0	5.0
K 14	*x*	*y*	136	5.0	3.3
K 15	*x*	*y*	136	3.3	5.0
K 16	*x*	*y*	136	3.3	3.3
K 17	*y*	*x*	68	5.0	5.0
K 18	*y*	*x*	68	5.0	3.3
K 19	*y*	*x*	68	3.3	5.0
K 20	*y*	*x*	68	3.3	3.3
K 21	*y*	*x*	136	5.0	5.0
K 22	*y*	*x*	136	5.0	3.3
K 23	*y*	*x*	136	3.3	5.0
K 24	*y*	*x*	136	3.3	3.3
K 25	*y*	*y*	68	5.0	5.0
K 26	*y*	*y*	68	5.0	3.3
K 27	*y*	*y*	68	3.3	5.0
K 28	*y*	*y*	68	3.3	3.3
K 29	*y*	*y*	136	5.0	5.0
K 30	*y*	*y*	136	5.0	3.3
K 31	*y*	*y*	136	3.3	5.0
K 32	*y*	*y*	136	3.3	3.3

TAB 1. Parameter configurations for uniaxial in-plane tension tests on structurally stitched carbon fiber NCF laminates

2.2. Tension tests

Unstitched and structurally stitched laminates were tension tested under uniaxial loading parallel to the *x* and *y* axes. 150 mm long and 20 mm wide coupon specimens were cut out of the cured [A1-B-A2] laminates with a water-cooled diamond saw. The specimens were tested in a servo-hydraulic Schenk PL 100 kN testing machine with a constant deformation rate of 2 mm/min until ultimate failure. Upon loading the force and the elongation in the loading direction were recorded from which the tensile strength and modulus were evaluated according to Airbus standards; [16], [17].

2.3. Micrograph examinations for void characterization

The insertion of a stitching yarn in the thickness direction results in a localized dislocation of the in-plane fibers and the formation of voids which mostly consist of pure resin after resin infusion. Both effects are responsible for the change of stiffness and strength properties in stitched laminates. Voids caused by stitching were analyzed by means of micrograph sections parallel to the laminate plane which were produced in each layer of the composite. FIG 3 shows a micrograph section of a -45°-layer with a large void consisting of the impregnated stitching yarn and an area of the pure resin. The majority of stitching voids are diamond-shaped with the longer axis oriented parallel to the fiber direction of the layer. Due to the small cross-sectional area of the yarns relative to the total area of the void the contribution of the yarn to the in-plane properties of the layer was neglected in contrast to the resin pocket. As the NCF binding yarns create similar voids but with a much lower area compared to structural stitching, voids caused by NCF binding yarns were neglected in the unit cell model for simplification. The periodicity of the structural stitching was represented in the model [12].

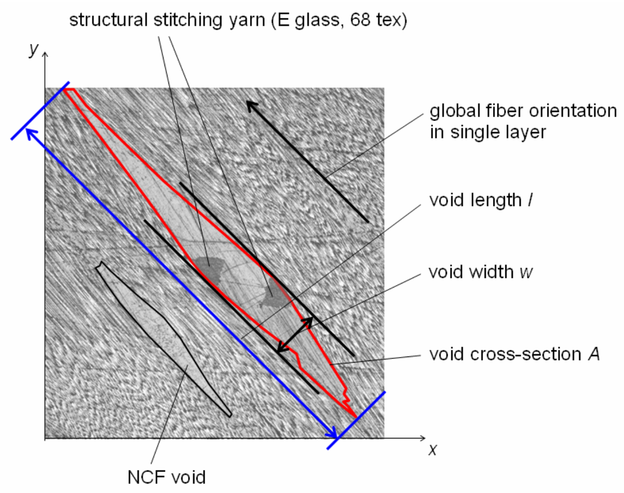

FIG 3. Micrograph section parallel to laminate plane of a -45° layer of a structurally stitched [A1-B-A2] CFRP laminate [12]

For all stitching configurations micrographs of four adjoining voids were produced and the void area, width and length (FIG 3) was measured from which the corresponding arithmetic means, standard deviations and the through-thickness distributions were determined, as given in [12]. The optical characterization of the voids resulting from structural stitching clearly revealed that the void cross-sectional area, width and length increase with an increasing yarn thickness and decrease from the top and bottom surfaces towards the center of the laminate.

3. UNIT CELL MODEL FOR STRUCTURALLY STITCHED NCF CFRP LAMINATES

3.1. Model definition

An ANSYS® finite element model based on a representative unit cell approach was developed to predict the elastic constants as well as the in-plane strength of structurally stitched NCF laminates. The parametric model is capable to consider the number, thickness and fiber orientation of the laminate layers, the cross-section area and width of stitching voids, the stitch spacing, pitch length and stitching direction as well as the loading direction.

FIG 4 shows an example of the unit cell models representing the parameter configurations K 1 and K 17. In each layer of the laminate a diamond-shaped central void with its major axis oriented parallel to the fiber direction of the layer and constant cross-section are modeled. The numerical values of the void area and width are determined from the corresponding thickness distributions of the micrograph analyses.

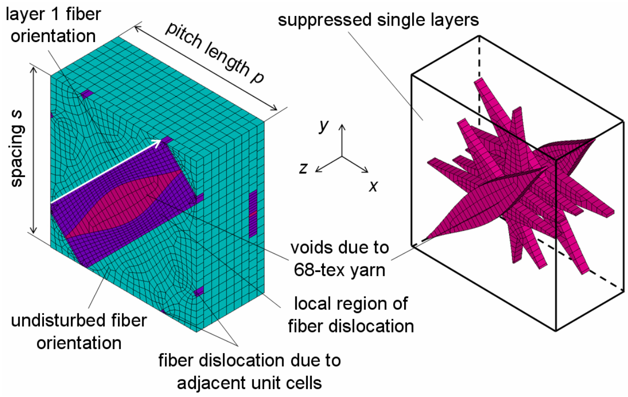

FIG 4. Unit cell model of a structurally stitched [A1-B-A2] CFRP laminate (parameter configurations K 1 and 17)

All elements of the unit cell model (undisturbed and disturbed NCF areas, resin pocket) are described by 3D 20-node SOLID186 elements providing quadratic displacement functions along the element edges and anisotropic material properties. The local regions of fiber dislocation in each layer were assumed to extend across a length and width equal to the mean length and twice the averaged width of the void. The local fiber orientation next to the void parallels the void orientation and decreases to the global fiber orientation along the outer contour of the disturbed area. Each finite element row in the fiber dislocation region area is defined by the element centers lining up along a cosine function in the global layer coordinate system. The fiber orientation in each finite element is defined by the derivative of the cosine function with respect to x at the element center [12]. Depending on the considered configuration, it may be necessary to include additional parts of voids and fiber dislocation regions from adjacent unit cells (FIG 4).

3.2. Material properties of single layer

The mechanical behavior of the void is described by the properties of the neat resin matrix. As discussed above the insertion of the stitching yarn may result in a global increase of the laminate thickness and a reduction of the fiber volume fraction. On the other hand, the in-plane fibers are dislocated laterally leading to an increased fiber volume content in the vicinity of the void because of the higher packing density of the fibers in comparison to the unstitched laminate. As a consequence, the fiber volume fraction not only changes from one parameter configuration to another, but also from layer to layer for a specific combination, which needs to be considered in the estimation of the elastic and the strength properties:

$$\varphi_{\text{stitched}} = \frac{t_{\text{unstitched}}}{t_{\text{stitched}}} \cdot \frac{p \cdot s}{p \cdot s - A_{\text{void}}} \cdot \varphi_{\text{unstitched}} \quad (1)$$

In (1) $\varphi_{\text{unstitched}}$, $\varphi_{\text{stitched}}$, $t_{\text{unstitched}}$, and t_{stitched} denote the fiber volume fraction and thickness of the unstitched and structurally stitched layer of the laminate, A_{void} is the cross-section of the void taking adjacent unit cells into account [12]. For simplification the fiber volume fraction of the individual layers of the laminate is assumed to be constant in the unit cell model.

To determine the elastic constants (Young's moduli $E_{\|}$, $E_{\perp}$, shear moduli $G_{\perp\|}$, $G_{\perp\perp}$, Poisson's ratios $\nu_{\perp\|}$, $\nu_{\perp\perp}$) of the undisturbed and disturbed NCF areas of each layer of the laminate a micro-mechanic approach is used. In the micro-mechanic models transversely isotropic and isotropic material behavior was assumed for the carbon fiber and the polymer matrix:

$$E_{\|} = E_{\text{f},\|} \cdot \varphi + (1-\varphi) \cdot E_{\text{m}} \quad (2)$$

$$\varphi = \varphi_{\text{stitched}} \quad (3)$$

$$E_{\perp} = \frac{E_{\text{f},\perp} \cdot E_{\text{m}}}{\varphi \cdot E_{\text{m}} + (1-\varphi) \cdot E_{\text{f},\perp}} \quad (4)$$

$$\nu_{\perp\|} = \nu_{\text{f},\perp\|} \cdot \varphi + (1-\varphi) \cdot \nu_{\text{m}} \quad (5)$$

$$\nu_{\perp\perp} = \nu_{\text{f},\perp\|} \cdot \varphi + (1-\varphi) \cdot \nu_{\text{m}} \cdot \frac{\left(1 + \nu_{\text{m}} - \nu_{\perp\|} \cdot \frac{E_{\text{m}}}{E_{\|}}\right)}{\left(1 - \nu_{\text{m}}^2 + \nu_{\text{m}} \cdot \nu_{\perp\|} \cdot \frac{E_{\text{m}}}{E_{\|}}\right)} \quad (6)$$

$$G_{\perp\|} = \frac{G_{\text{m}} \cdot G_{\text{f},\perp\|}}{G_{\text{f},\perp\|} \cdot (1-\varphi) + G_{\text{m}} \cdot \varphi} \quad (7)$$

$$G_{\text{m}} = \frac{E_{\text{m}}}{2 \cdot (1+\nu_{\text{m}})} \quad (8)$$

$$G_{\perp\perp} = \frac{E_{\|}}{2 \cdot (1+\nu_{\perp\perp})} \quad (9)$$

In these equations E, G and ν are the Young's modulus, shear modulus and Poisson's ratio of the fiber (index f) and matrix (index m), respectively, as listed in TAB 2.

Due to the lack of experimental results for the considerably varying fiber volume fractions the strength properties (tensile: $R_{\|}^{t}$, $R_{\perp}^{t}$, compressive: $R_{\|}^{c}$, $R_{\perp}^{c}$, shear: $R_{\perp\|}$) of the undisturbed and disturbed NCF areas are estimated by micro-mechanic models [18] and correlated to experimental results (TAB 2) for a fiber volume fraction of 0.6 (index $\varphi = 0.6$) by correction terms denoted by the index corr.

The tensile and compressive strengths $R_{\|}^{t}$ and $R_{\|}^{c}$ parallel to the fiber direction

$$R_{\|}^{t} = \left(E_{\text{f},\|} \cdot \varphi + (1-\varphi) \cdot E_{\text{m}}\right) \cdot \varepsilon_{\min} \cdot R_{\|,\text{corr}}^{t} \quad (10)$$

$$R_{\|}^{c} = \frac{\left(E_{\text{f},\|} \cdot \varphi + (1-\varphi) \cdot E_{\text{m}}\right) \cdot \left(1 - \varphi^{\frac{1}{3}}\right) \cdot \varepsilon_{\min}}{\nu_{\perp\|} \cdot \varphi + (1-\varphi) \cdot \nu_{\text{m}}} + R_{\|,\text{corr}}^{c} \quad (11)$$

can be determined by

$$\varepsilon_{\min} = \min\left\{\varepsilon_{\text{f},\|,\text{ult}}^{t}, \varepsilon_{\text{m}}\right\} \quad (12)$$

from the minimum of the fiber fracture strain $\varepsilon_{\text{f},\|,\text{ult}}^{t}$ under tension loading or the ultimate tension strain ε_{m} of the matrix and the correction terms

$$R_{\|,\text{corr}}^{t} = \frac{R_{\|,\varphi=0.6}^{t}}{\left(E_{\text{f},\|} \cdot 0.6 + (1-0.6) \cdot E_{\text{m}}\right) \cdot \varepsilon_{\min}} \quad (13)$$

$$R_{\|,\text{corr}}^{c} = R_{\|,\varphi=0.6}^{c} - \frac{\left(E_{\text{f},\|} \cdot 0.6 + (1-0.6) \cdot E_{\text{m}}\right) \cdot \left(1 - 0.6^{\frac{1}{3}}\right) \cdot \varepsilon_{\min}}{\nu_{\perp\|} \cdot 0.6 + (1-0.6) \cdot \nu_{\text{m}}} \quad (14)$$

HTA carbon fiber (transversely isotropic)		**RTM 6 epoxy matrix (isotropic)**		**unidirectionally reinforced layer (transversely isotropic)**	
Young's modulus $E_{\text{f},\|}$ parallel to fiber direction [GPa]	246	Young's modulus E_{m} [MPa]	2890	tensile strength $R_{\|,\varphi=0.6}^{t}$ parallel to fiber direction [MPa]	1995
Young's modulus $E_{\text{f},\perp}$ perpendic. to fiber direction [GPa]	28	shear modulus G_{m} [MPa]	1070	compr. strength $R_{\|,\varphi=0.6}^{c}$ parallel to fiber direction [MPa]	1499
shear modulus G_{f} [GPa]	50	Poisson's ratio ν_{m} [1]	0.35	tensile strength $R_{\perp,\varphi=0.6}^{t}$ perpendic. to fiber direction [MPa]	52
Poisson's ratio ν_{f} [1]	0.23	ultimate tension strain ε_{m} [%]	3.4	compr. strength $R_{\perp,\varphi=0.6}^{c}$ perpendic. to fiber direction [MPa]	240
ultimate tension strain $\varepsilon_{\text{f},\|,\text{ult}}^{t}$ parallel to fiber direction [%]	1.7	min. strength $R_{\perp,\min}^{t,c} = R_{\text{m}}$ perpendic. to fiber direction [MPa]	75	shear strength $R_{\perp\|,\varphi=0.6}$ [MPa]	62
		min. shear strength $R_{\perp\|,\min} = R_{\text{m},21}$ [MPa]	43		

TAB 2. Mechanical properties of HTA carbon fiber, RTM 6 epoxy matrix and unidirectionally reinforced layer (fiber volume fraction 0.6)

The strength values $R_\perp^{\,t}$ and $R_\perp^{\,c}$ perpendicular to the fiber direction are calculated from:

(15) $$R_\perp^{\,t} = \left(1 + \left(\varphi - \sqrt{\varphi}\right)\cdot\left(1 - \frac{E_\mathrm{m}}{E_{\mathrm{f},\perp}}\right)\right)\cdot R_{\perp,\,\mathrm{min}}^{\,t} + R_{\perp,\,\mathrm{corr}}^{\,t}$$

(16) $$R_\perp^{\,c} = \left(1 + \left(\varphi - \sqrt{\varphi}\right)\cdot\left(1 - \frac{E_\mathrm{m}}{E_{\mathrm{f},\perp}}\right)\right)\cdot R_{\perp,\,\mathrm{min}}^{\,c}\cdot C + R_{\perp,\,\mathrm{corr}}^{\,c}$$

(17) $$R_{\perp,\,\mathrm{min}}^{\,t,c} = \min\left\{ R_{\mathrm{f},\perp}^{\,t,c}, R_\mathrm{m}\right\}$$

(18) $$R_{\perp,\,\mathrm{corr}}^{\,t} = R_{\perp,\varphi=0.6}^{\,t} - \left(1 + \left(0.6 - \sqrt{0.6}\right)\cdot\left(1 - \frac{E_\mathrm{m}}{E_{\mathrm{f},\perp}}\right)\right)\cdot R_{\perp,\,\mathrm{min}}^{\,t}$$

(19) $$R_{\perp,\,\mathrm{corr}}^{\,c} = R_{\perp,\varphi=0.6}^{\,c} - \left(1 + \left(0.6 - \sqrt{0.6}\right)\cdot\left(1 - \frac{E_\mathrm{m}}{E_{\mathrm{f},\perp}}\right)\right)\cdot R_{\perp,\,\mathrm{min}}^{\,c}\cdot C$$

(20) $$C = 1 - \left(\frac{4\cdot 0.005}{(1-\varphi)\cdot\pi}\right)^{\frac{1}{2}}$$

where $R_{\perp,\,\mathrm{min}}^{\,t,\,c}$ is the minimum of the transverse fiber strength $R_{\mathrm{f},\,\perp,}^{\,t,\,c}$ under tension/compression loading or the matrix strength R_m. In these equations the factor C describes the stress magnification due to a void inclusion with a volume content of 0.005.

The shear strength $R_{\perp\parallel}$ is determined by

(21) $$R_{\perp\parallel} = \left(1 + \left(\varphi - \sqrt{\varphi}\right)\cdot\left(1 - \frac{G_\mathrm{m}}{G_{\mathrm{f},\perp\parallel}}\right)\right)\cdot R_{\perp\parallel,\mathrm{min}}\cdot C + R_{\perp\parallel,\,\mathrm{corr}}$$

(22) $$R_{\perp\parallel,\mathrm{min}} = \min\left\{ R_{\mathrm{f},\perp\parallel}, R_{\mathrm{m},21}\right\}$$

(23) $$R_{\perp\parallel,\mathrm{corr}} = R_{\perp\parallel,\varphi=0.6} - \left(1 + \left(0.6 - \sqrt{0.6}\right)\cdot\left(1 - \frac{G_\mathrm{m}}{G_{\mathrm{f},\perp\parallel}}\right)\right)\cdot R_{\perp\parallel,\mathrm{min}}\cdot C \quad ,$$

in which $R_{\perp\parallel,\,\mathrm{min}}$ is the minimum of the fiber or the matrix shear strength $R_{\mathrm{f},\,\perp\parallel}$ and $R_{\mathrm{m},\,\perp\parallel}$.

3.3. Elastic constants of laminate

FIG 5 illustrates the process to determine the elastic constants of stitched laminates. To estimate the elastic behavior of structurally stitched laminates with arbitrary lay-up their mechanical behavior can be modeled as a combination of a membrane and a plate element. Hence, the unit cell model must satisfy the stress-strain relation of a laminated composite element with the global stiffness matrix $[\mathbf{ABD}]$:

(24) $$[\mathbf{ABD}] = \begin{bmatrix} [\mathbf{A}] & [\mathbf{B}] \\ [\mathbf{B}] & [\mathbf{D}] \end{bmatrix}$$

The in-plane Young's moduli E_x and E_y, the shear modulus G_{xy} and the Poisson's ratios ν_{yx} and ν_{xy} of the stitched laminate can be determined from the coefficients of the global compliance matrix $[\mathbf{ABD}]^{-1}$:

(25) $$[\mathbf{ABD}]^{-1} = \begin{bmatrix} \left[\mathbf{A}^*\right] & \left[\mathbf{B}^*\right] \\ \left[\mathbf{B}^*\right]^\mathrm{T} & \left[\mathbf{D}^*\right] \end{bmatrix}$$

and the laminate thickness t by

(26) $$E_x = \frac{1}{A_{11}^*\cdot t}$$

(27) $$E_y = \frac{1}{A_{22}^*\cdot t}$$

(28) $$G_{xy} = \frac{1}{A_{66}^*\cdot t}$$

(29) $$\nu_{yx} = -\frac{A_{12}^*}{A_{11}^*}$$

(30) $$\nu_{xy} = -\frac{A_{21}^*}{A_{22}^*}$$

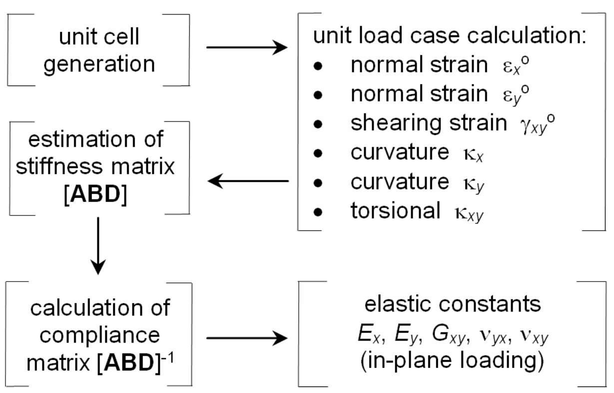

FIG 5. Flowchart for the determination of elastic constants of structurally stitched NCF laminates [12]

3.4. Laminate strength

Within the last decades continuum mechanics based failure theories for homogenized single layers in multidirectional laminates were developed. According to Puck [19], such a failure analysis has to include the three components strain and stress analysis, fracture analysis and degradation analysis. As this kind of failure models are missing in commercial FE programs, a module was developed, which enables the strength prediction of stitched laminates taking the aforementioned components into account (FIG 6).

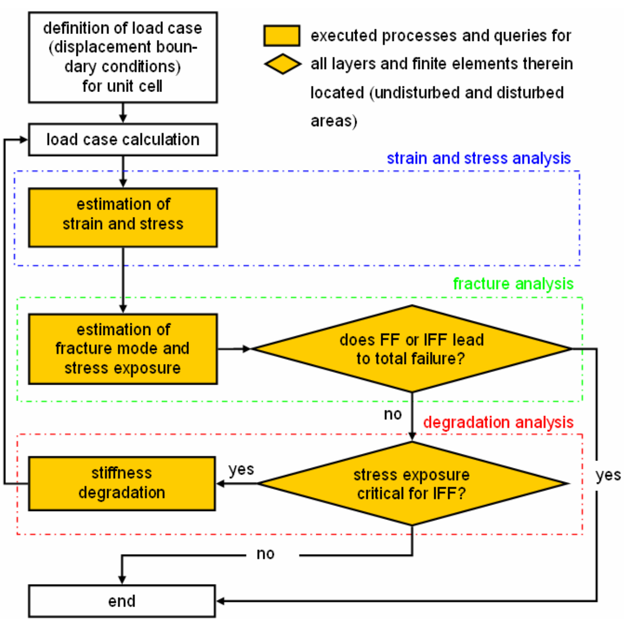

FIG 6. Flowchart for layer-by-layer fracture analysis with the components strain and stress, fracture and degradation analysis adapted to the FE program

3.4.1. Fracture analysis

In unidirectionally (UD) reinforced layers two extremely different failure types occur; i. e. fiber fracture (FF) and inter-fiber fracture (IFF). Therefore, the fracture analysis needs to distinguish these two phenomena by individual failure criteria. Mathematically, fracture conditions can be described by means of the stress exposure f_E, which describes the load for a given stress or stress combination in comparison to the maximum sustainable stress state.

3.4.1.1. Fiber fracture

FF is to be understood as a fracture of a large amount of elementary fiber filaments causing the loss of the load bearing capacity of a macroscopic area in the fiber direction [20]. To estimate the FF stress exposure the maximum stress criterion was applied:

(31) $\sigma_1 > 0: \qquad f_E = \dfrac{\sigma_1}{R_\parallel^t}$

(32) $\sigma_1 \le 0: \qquad f_E = \dfrac{|\sigma_1|}{R_\parallel^c}$

3.4.1.2. Inter-fiber fracture

IFF are macroscopic cracks parallel to the fiber direction running through the total thickness of the layer which are partly caused by cohesive failure of the matrix or partly induced by adhesive failure of the fiber/matrix interface. The main advantage of Puck's IFF action-plane criterion for 3D stress states is the possibility to distinguish between uncritical and critical (leading to total failure of the laminate) IFF and to determine the direction of the fracture plane (fp) by means of the fracture angle θ_{fp} ($-90° \le \theta_{fp} \le +90°$); FIG 7. To determine the fracture plane the stress components σ_n, τ_{nt} and τ_{n1} which act in the fracture plane and initiate IFF are calculated by transforming the UD layer stress components σ_2, σ_3, τ_{32}, τ_{31} and τ_{21}:

(33) $$\begin{Bmatrix}\sigma_n\\ \tau_{nt}\\ \tau_{n1}\end{Bmatrix} = \begin{bmatrix} c^2 & s^2 & 2cs & 0 & 0\\ -sc & sc & (c^2-s^2) & 0 & 0\\ 0 & 0 & 0 & s & c\end{bmatrix} \cdot \begin{Bmatrix}\sigma_2\\ \sigma_3\\ \tau_{23}\\ \tau_{31}\\ \tau_{21}\end{Bmatrix}$$

with $c = \cos\theta$ and $s = \sin\theta$.

The stress exposure which is depending on θ was estimated by equations (34) and (35), in which the stress components $\sigma_n^{t,c}$, τ_{nt} and τ_{n1} are related to the strength values $R_\perp^{t,c}$ and $R_{\perp\parallel}$ as well as the action-plane fracture resistance $R_{\perp\perp}^A$. In general, crack assisting tensile ($\sigma_n > 0$) and crack impeding compressive stresses ($\sigma_n < 0$) transverse to the fiber direction must be distinguished in the IFF criterion:

(34) $\sigma_n \ge 0$:

$$f_E(\theta) = \sqrt{\left[\left(\frac{1}{R_\perp^t} - \frac{p_{\perp\psi}^t}{R_{\perp\psi}^A}\right)\cdot\sigma_n\right]^2 + \left(\frac{\tau_{nt}}{R_{\perp\perp}^A}\right)^2 + \left(\frac{\tau_{n1}}{R_{\perp\parallel}}\right)^2} + \frac{p_{\perp\psi}^t}{R_{\perp\psi}^A}\cdot\sigma_n$$

(35) $\sigma_n < 0$:

$$f_E(\theta) = \sqrt{\left(\frac{\tau_{nt}}{R_{\perp\perp}^A}\right)^2 + \left(\frac{\tau_{n1}}{R_{\perp\parallel}}\right)^2 + \left(\frac{p_{\perp\psi}^c}{R_{\perp\psi}^A}\cdot\sigma_n\right)^2} + \frac{p_{\perp\psi}^c}{R_{\perp\psi}^A}\cdot\sigma_n$$

where

(36) $\dfrac{p_{\perp\psi}^{t,c}}{R_{\perp\psi}^A} = \dfrac{p_{\perp\perp}^{t,c}}{R_{\perp\perp}^A}\cdot\cos^2\psi + \dfrac{p_{\perp\parallel}^{t,c}}{R_{\perp\parallel}}\cdot\sin^2\psi$

(37) $\cos^2\psi = 1 - \sin^2\psi = \dfrac{\tau_{nt}^2}{\tau_{nt}^2 + \tau_{nl}^2}$

(38) $p_{\perp\perp}^t = p_{\perp\perp}^c = \dfrac{1}{2}\cdot\left(\sqrt{1 + 2\cdot p_{\perp\parallel}^c \cdot \dfrac{R_\perp^c}{R_{\perp\parallel}}} - 1\right)$

(39) $R_{\perp\perp}^A = \dfrac{R_\perp^c}{2\cdot\left(1 + p_{\perp\perp}^c\right)}$

The meaning of the parameters introduced in eqs. (34) through (39) is outlined in FIG 8 and FIG 9. If no experimental data are available for the slope parameters $p_{\perp\parallel}^t$ and $p_{\perp\parallel}^c$ the numbers 0.35 and 0.30 are recommended for CFRP [19]. Introducing the fracture condition $f_E(\theta) = 1$ into eqs. (34) and (35) results in the mathematical formulation of the master fracture body in (σ_n, τ_{nt}, τ_{n1}) space, as shown in FIG 8.

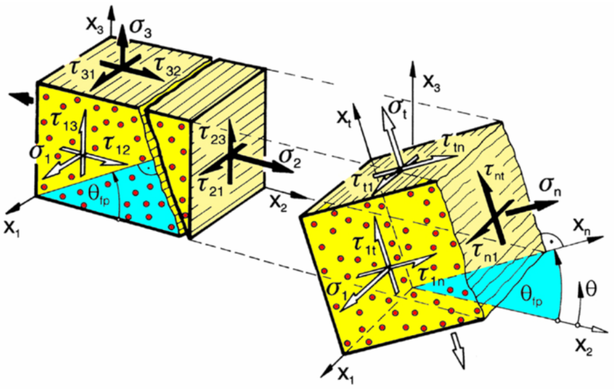

FIG 7. Determination of fiber parallel fracture plane and fracture angle θ_{fp} by transformation of the UD layer stress components σ_2, σ_3, τ_{32}, τ_{31} and τ_{21} into the fracture plane stress components σ_n, τ_{nt} and τ_{n1} [19]

Depending on the stress combination in the fracture plane four IFF modes A, A*, B and C must be distinguished. Mode A is caused by a transverse tensile stress σ_n^t, a shear stress τ_{n1} or a combination of both. If additionally a shear stress τ_{nt} acts the IFF is classified as mode A*. In case of mode B a transverse compressive stress σ_n^c acts together with a shear stress τ_{n1}. In a multi-directional laminate these IFF modes do not directly initiate the total failure of the laminate. Mode C characterizes an IFF mode which acts in a fracture plane inclined at the fracture angle $\theta_{fp} \ne 0°$. This critical mode is caused by a combination of the stresses σ_n^c, τ_{n1} and τ_{nt} which may cause total failure of the laminate due to wedge effects. Referring to Puck this effect can only occur if the fractured layer is relatively thick and is combined with high fracture angles (±30° to ±45°) and stress exposures $f_E \ge 1.25$ ([19], [22]).

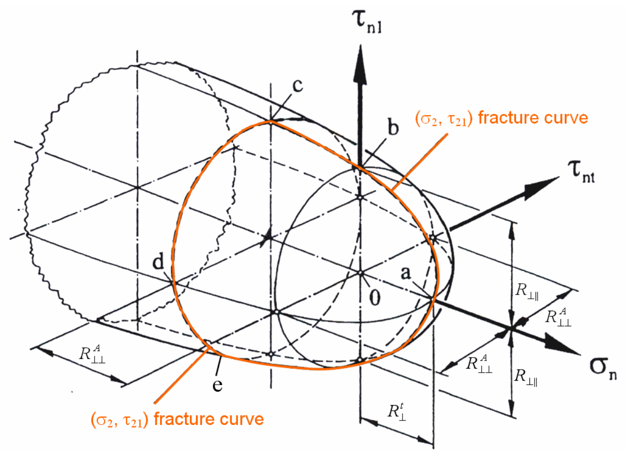

FIG 8. Master fracture body in (σ_n, τ_{nt}, τ_{n1}) stress space for σ_1 = 0 with fracture limit surfaces and fracture curves for Puck's action-plane criterion [21]. For a plane stress state ($\sigma_n = \sigma_2$, $\tau_{n1} = \tau_{21}$) the (σ_2, τ_{21}) fracture curve follows the lines from a to e.

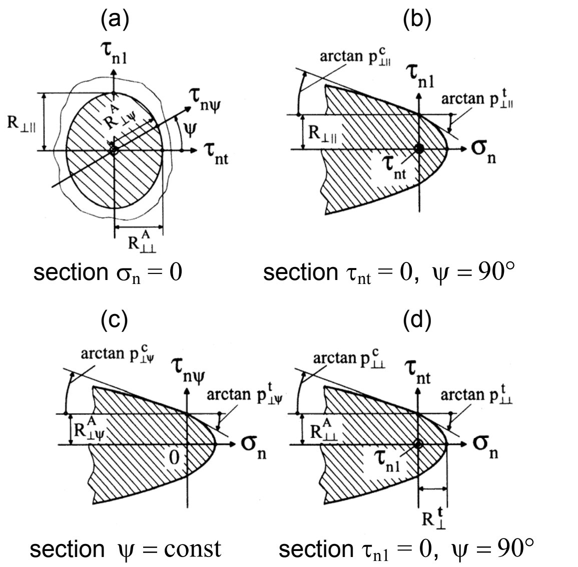

FIG 9. Definition of action-plane fracture resistance $R_{\perp\psi}^A$ and gradients $p_{\perp\parallel}^{(t,c)}$, $p_{\perp\psi}^{(t,c)}$ and $p_{\perp\perp}^{(t,c)}$ as given in equations (34) to (39) [20]

3.4.2. Degradation analysis

Uncritical IFF modes A, A* and B as well as mode C for small fracture angles (-30° < θ_{fp} < +30°) and moderate stress exposures ($f_E < 1.25$) reduce the contribution of the affected layers to the load-bearing of the laminate. In the context of the continuum mechanics the post-failure behavior of uncritical IFF modes can be modeled by stiffness degradation for which a Chiu model was modified to account for 3D stress states. The used Chiu model describes IFF damage processes with $f_E > 1$ by means of an immediate degradation of the elastic constants $E_{n,\,deg}$, $G_{n1,\,deg}$, $G_{t1,\,deg}$ and $G_{nt,\,deg}$ of the fracture plane to a residual value. Usually, the stiffness degradation leads to a complete relocation of stresses from the layer affected by IFF into neighboring layers and, hence, provides a conservative strength forecast.

In case of modes A and A* opening IFF cracks driven by σ_n^t are induced. Although the acting stresses σ_n^t, τ_{n1} and τ_{nt} can no longer be transferred across the crack surfaces a certain residual load bearing capacity between the cracks is retained which is modeled by a non-zero residual stiffness, as recommended in [23]:

$$(40)\quad \begin{pmatrix} E_{n,\deg} \\ G_{n1,\deg} \\ G_{t1,\deg} \\ G_{nt,\deg} \end{pmatrix} = \begin{pmatrix} 0.03 \cdot E_n \\ 0.67 \cdot G_{n1} \\ 0.67 \cdot G_{t1} \\ 0.67 \cdot G_{nt} \end{pmatrix} .$$

According to [24] the Poisson's ratios are not affected by IFF cracks and are kept constant consequently.

In the case of mode B or uncritical mode C cracking transverse compressive stresses σ_n^c can be transferred across the crack surfaces. Therefore, only the shear moduli are reduced as a consequence of the IFF cracking:

$$(41)\quad \begin{pmatrix} E_{n,\deg} \\ G_{n1,\deg} \\ G_{t1,\deg} \\ G_{nt,\deg} \end{pmatrix} = \begin{pmatrix} E_n \\ 0.67 \cdot G_{n1} \\ 0.67 \cdot G_{t1} \\ 0.67 \cdot G_{nt} \end{pmatrix} .$$

After reducing the stiffness properties relative to the fracture plane, as given in eqs. (40) and (41), the reduced coefficients of the compliance matrix

$$(42)\quad [\mathbf{S}_{\deg}] = \begin{bmatrix} \frac{1}{E_1} & -\frac{\nu_{1n}}{E_n} & -\frac{\nu_{1t}}{E_t} & 0 & 0 & 0 \\ & \frac{1}{E_{n,\deg}} & -\frac{\nu_{nt}}{E_t} & 0 & 0 & 0 \\ & & \frac{1}{E_t} & 0 & 0 & 0 \\ & & & \frac{1}{G_{nt,\deg}} & 0 & 0 \\ & \text{symm.} & & & \frac{1}{G_{t1,\deg}} & 0 \\ & & & & & \frac{1}{G_{n1,\deg}} \end{bmatrix}$$

has to be transformed into the $(1, 2, 3)$ coordinate system of the UD layer:

$$(43)\quad [\overline{\mathbf{S}_{\deg}}] = [\,\mathbf{T}\,]^{\mathrm{T}} \cdot [\mathbf{S}_{\deg}] \cdot [\,\mathbf{T}\,]$$

with

$$(44)\quad [\mathbf{T}] = \begin{bmatrix} 1 & 0 & 0 & 0 & 0 & 0 \\ 0 & c^2 & s^2 & 2cs & 0 & 0 \\ 0 & s^2 & c^2 & -2cs & 0 & 0 \\ 0 & cs & -cs & (c^2 - s^2) & 0 & 0 \\ 0 & 0 & 0 & 0 & c & -s \\ 0 & 0 & 0 & 0 & s & c \end{bmatrix} .$$

From the coefficients of $[\overline{\mathbf{S}_{\deg}}]$ the reduced elastic constants of the UD layer can be determined and allocated to the corresponding finite element.

3.4.3. Boundary conditions and loading

Load cases and displacement boundary conditions as described in TAB 3 and FIG 10 were used to estimate the strength of the stitched laminates under tension loading in *x* or *y* direction. Starting from $\varepsilon^t_{x,\,\mathrm{ult}} = 0.01$ or $\varepsilon^t_{y,\,\mathrm{ult}} = 0.01$ the strain loading is increased (or decreased) in each iteration step until FF or a critical mode C IFF is predicted with an accuracy of $\pm 0.5\,\%$ ($f_{\mathrm{E}} = 1$ or $f_{\mathrm{E}} = 1.25$). Finally, the tensile strength components R^t_x or R^t_y are determined as the sum of the absolute values of all nodal forces acting on surfaces s1 and s3 (loading in *x* direction) or *s*2 and *s*4 (loading in *y* direction) divided by the area of the corresponding surfaces.

loading direction	load case	coordinate system	surface / coordinate	displacement boundary conditions at unit cell surfaces
x	$\varepsilon_x = \varepsilon^t_{x,\,\mathrm{ult}}$, $\varepsilon_y = -\varepsilon^t_{x,\,\mathrm{ult}} \cdot \nu_{yx}$	*cs*1	*s*1, *s*2, *s*3, *s*4	$u_x(x) = \varepsilon_x \cdot x$, $u_y(y) = \varepsilon_y \cdot y$
			$x = y = z = 0$	$u_z(x, y, z) = 0$
y	$\varepsilon_y = \varepsilon^t_{y,\,\mathrm{ult}}$, $\varepsilon_y = -\varepsilon^t_{x,\,\mathrm{ult}} \cdot \nu_{yx}$	*cs*2	*s*1, *s*2, *s*3, *s*4	$u_y(y) = \varepsilon_y \cdot y$, $u_x(x) = \varepsilon_x \cdot x$
			$x = y = z = 0$	$u_z(x, y, z) = 0$

TAB 3. Boundary conditions u_x, u_y and u_z on unit cell surfaces corresponding to strain loading in *x* and *y* (s. FIG 10 for reference coordinate systems *cs* and surfaces *s*)

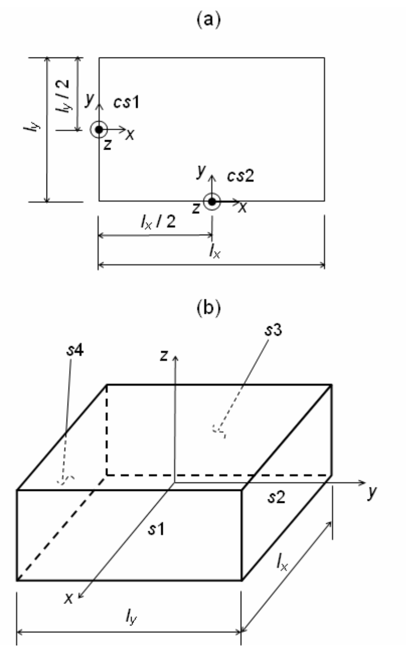

FIG 10. (a) Reference coordinate systems *cs*1 and *cs*2, lengths l_x and l_y
(b) surfaces $s_1 \ldots s_4$ for definition of boundary conditions on the surfaces of the unit cell model (TAB 3), origin of all reference coordinate systems located in the mid-plane of the unit cell ($z_{cs1} = z_{cs2} = z = 0$)

4. COMPARISON OF EXPERIMENTAL AND ANALYTICAL RESULTS

To demonstrate the influence of through-thickness stitching of NCF laminates on the in-plane tensile strength, the results of the structurally stitched CFRP laminates are normalized with the corresponding property of the unstitched laminate. In general, structural stitching reduces the tensile strength of CFRP laminates. The experimental investigation of the stitched [A1-B-A2] CFRP laminates showed a maximum reduction of the in-plane tensile strength amounting to 36 % compared to the unstitched laminate (FIG 11, parameter configuration K 14; cf. TAB 2). Except of the configurations K 29, K 30 and K 31, the application of a 136 tex stitching yarn caused a larger strength reduction compared to a 68 tex yarn. A 3 % and 4 % increase of the tensile strength was determined for K 25 and K 26, respectively. In stitched laminates with configurations K 4, K 18 and K 27 no influence on the tensile strength could be observed.

The experimental results were used to validate the failure analysis in the unit cell model. The numerical results revealed that the reduction of the in-plane tensile strength of [A1-B-A2] CFRP laminates due to structural stitching can be simulated. Under tension loading in *x* direction the theoretically determined strength was lower compared to the experiments except of the configurations K 14 – K 16. The maximum overestimation and underestimation of the tensile strength was about 17 % (K 3) and 12 % (K 15), respectively. However, for the loading direction *y* the FE unit cell mostly overestimated the experiment (except of K 18, K 22 and K 31). The maximum overestimation of the tensile strength was in the order of 18 % (K 21), the maximum underestimation was 9 % (K 18).The averaged discrepancy of the calculated results from the experimental data was about 8 %.

The underestimation of the tensile strength in *x* direction may be explained by the difference of the real fracture mechanism compared to the theoretical failure analysis. In reality the macroscopic failure of a complete layer is initialized by the simultaneous fracture of a large amount of elementary fibers only but a residual bearing capacity may be obtained in multi-directional laminates despite of a fiber fracture [19]. In the FE based failure analysis the total failure of the laminate is defined by the first occurrence of a fiber fracture in one finite element whereas stress relocation and further load increase are rejected. Normally this leads to a conservative forecast. In the analyzed laminates the first local fiber fracture in one element was always determined in layers oriented parallel to the loading direction at the largest width of the void.

The overestimation of the predicted strength under tensile loading in *y* direction may be attributed to the implementation of too high tensile strength values parallel to the fiber direction. In addition, the discrepancy may again be correlated with differences of the real fracture mechanisms compared to the failure analysis. Experiments on unstitched [A1-B-A2] laminates carried out lately revealed that initial IFFs in layers perpendicular to the loading direction (0° layers) directly cause IFFs in the neighboring ±45° layers. Therefore, one single load-bearing 90° layer located in the center of the laminate remains which may be subjected to pre-damage due to the IFF cracking in the

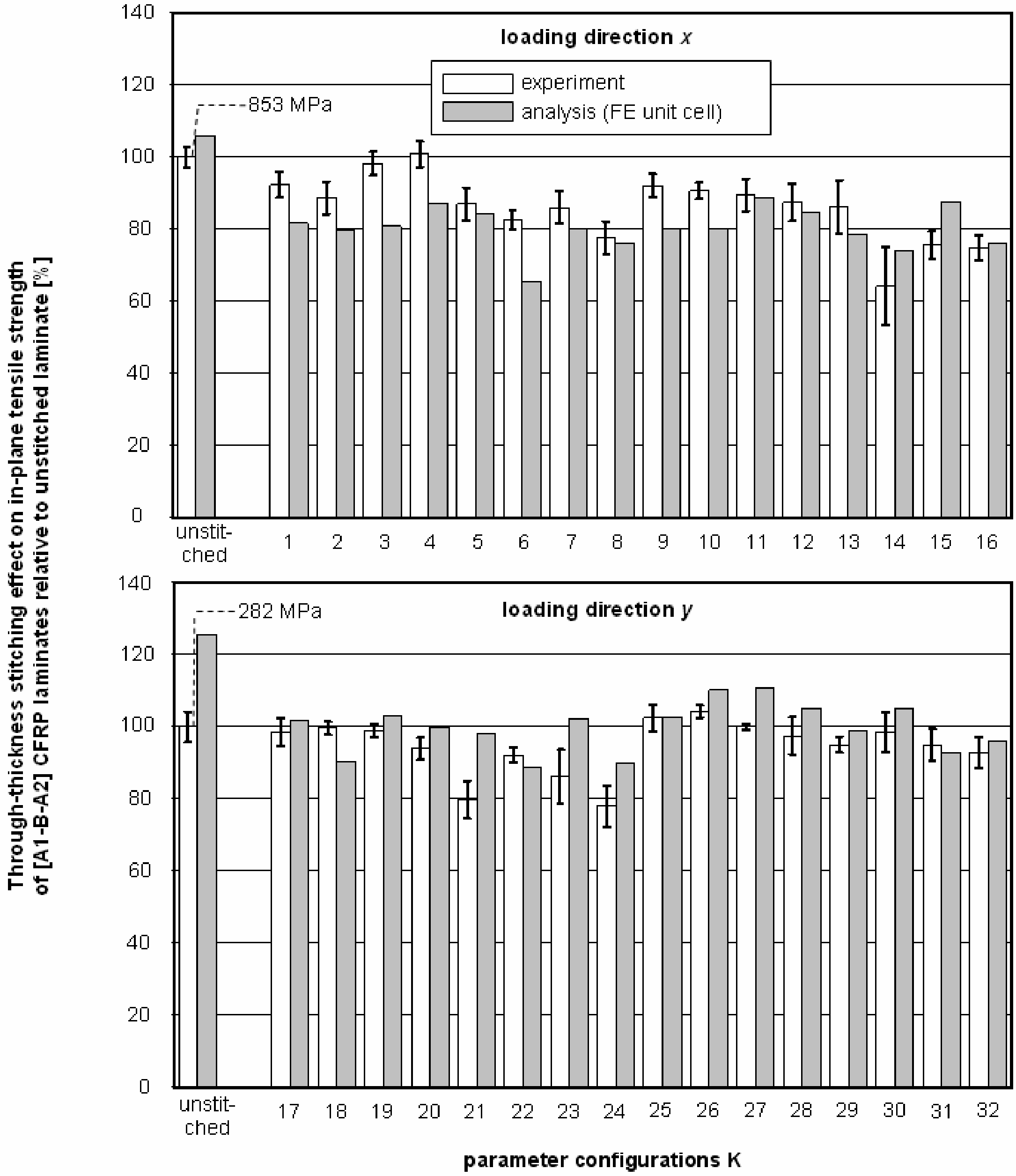

FIG 11. In-plane tensile strength of unstitched and stitched [A1-B-A2] CFRP laminates determined experimentally and theoretically, loading direction *x* and *y*

other layers leading to a significant strength reduction in this layer.

However, in the FE failure analysis initial IFFs occur in the 0° layers which are followed by stress relocation and further load increase in the ±45° layers without directly leading to IFF there. In addition, a potential pre-damage and strength reduction of the 90° layer can not be modeled by the FE failure analysis. This argument is supported by the fact that the strength of the unstitched laminate is overestimated by nearly 25 % in the analysis (cf. FIG 11).

5. CONCLUSION

Unstitched and structurally stitched [A1-B-A2] CFRP NCF laminates were investigated experimentally under in-plane tensile loading. It was observed that the loading direction and the stitching parameters (yarn thickness, spacing, pitch length and stitching direction) partially lead to a reduction of the in-plane tensile strength by up to 36 % compared to the unstitched laminate. In contrast to this result, a reduction of the strength can be avoided with a proper selection of the stitching parameters.

Micrograph investigations revealed that resin pockets and local fiber dislocations are caused by through-thickness stitching. To estimate the in-plane stiffness coefficients and strengths of structurally stitched [A1-B-A2] laminates the void geometry was determined in each layer of the laminate.

A finite element based unit cell model was developed to estimate the in-plane strength properties of 3D stitched NCF carbon fiber laminates depending on the number, thickness and fiber orientation of the layers, the void cross-section and width, the stitch spacing, pitch length and stitching direction as well as the loading direction. In the model local changes of the fiber volume fraction as well as regions with undisturbed and disturbed fiber orientations within the laminate layers are taken into account. The non-linear, continuum mechanics based failure analysis includes strain and stress analysis, fracture analysis and degradation analysis. For fiber failure the maximum stress criterion, for inter-fiber failure Puck's action plane criterion for 3D stress state are used to estimate the stress exposure. Post-failure behavior is modeled by partial stiffness degradation according to a Chiu model which was modified for 3D stress states.

Using this model the strength of stitched and unstitched laminates was analyzed for all parameter configurations included in the experimental study and validated against the experimental results. The comparison of experimental and numerical results showed that the strength of stitched laminates can be estimated with reasonable accuracy by means of the unit cell model. The mean deviation between the simulation and experiment results was 8 % with individual deviations up to 18 %.

6. REFERENCES

[1] Harris C E, Starnes J H, Shuart M J. An Assessment of the State-of-the-Art in the Design and Manufacturing of Large Composite Structures for Aerospace Vehicles, paper NASA/TM-2001-210844 NASA Langley Research Center, Hampton, Virginia, USA: 2001. http://techreports.Larc.NASA.gov/ltrs/.

[2] Weimer C, Preller T, Mitschang P, Drechsler K. Approach to net-shape preforming using textile technologies. Part I: Edges. Composites Part A 2000; 31: 1261–1268.

[3] Weimer C, Preller T, Mitschang P, Drechsler K. Approach to net-shape preforming using textile technologies. Part II: Holes. Composites Part A 2000; 31: 1269–1277.

[4] Dexter H B, Funk J G. Impact resistance and interlaminar fracture toughness of through-the-thickness reinforced graphite/epoxy, paper 86-CP1996, American Institute of Aeronautics and Astronautics, New York, USA: 1996, p. 700–709.

[5] Dransfield K A, Jain L K, Mai Y W. On the effects of stitching in CFRPs – I. Mode-I delamination toughness. Composites Science and Technology 1998; 58: 815–827.

[6] Wood M D K, Sun X, Tong L, Katzos A, Rispler A R, Mai Y W. The effect of stitch distribution on Mode I delamination toughness of stitched laminated composites – experimental results and FEA simulation. Composites Science and Technology 2007; 67: 1058–1072.

[7] Loendersloot, R., Lomov, S.V. Akkerman, R., Verpoest, I. "Carbon composites based on multiaxial multiply stitched preforms. Part 5: Geometry of sheared biaxial fabrics" Composites part A, 37 (2006), pp. 103 – 113.

[8] Lomov S V, Belov E B, Bischoff T, Ghosh S B, Truong Chi T, Verpoest I. Carbon composites based on multiaxial multiply stitched preforms. Part 1: Geometry of the preform. Composites Part A 2002; 33: 1171–1183.

[9] Truong Chi T, Vettori M, Lomov S V, Verpoest I. Carbon composites based on multi-axial multi-ply stitched preforms. Part 4: Mechanical properties of composites and damage observation. Composites Part A 2005; 36: 1207–1221.

[10] Mouritz A P, Cox B N. A mechanistic approach to the properties of stitched laminates. Composites Part A 2000; 31: 1–27.

[11] Roth Y C, Himmel N. Stitched Non-Crimp Fabric Laminates. From Manufacturing to In-plane Properties. Proceedings "14th International Conference on Composite Materials ICCM-11", June 14–18 2003, San Diego, CA, USA.

[12] Heß H, Roth Y C, Himmel N. Elastic constants estimation of stitched NCF CFRP laminates based on a finite element unit-cell model. Composites Science and Technology 2007; 67: 1081–1095.

[13] Dow M B, Dexter H B. Development of stitched, braided and woven composite structures in the ACT program and at Langley Research Center (1985–1997), NASA/TP-97-206234, NASA Langley Research Center, Hampton, Virginia, USA, 1997.

[14] Hörsting K. Rationalisierung der Fertigung langfaserverstärkter Verbundwerkstoffe durch den Einsatz multiaxialer Gelege. Aachen, Germany, 1994.

[15] Brandt J, Drechsler K, Filsinger J. Development trends in textile reinforcements for composites, 5th Japan International Symposium & Exhibition, Tokyo, Japan, 1997.

[16] Daimler-Benz-Aerospace Airbus. QVA-Z10-46-35, Bestimmung von Zugeigenschaften von CFK-Laminaten aus unidirektionalem Prepreg (Tape), Prüfung senkrecht zur Faser (90°), 1996.

[17] Daimler-Benz-Aerospace Airbus. QVA-Z10-46-36, Bestimmung von Zugeigenschaften von CFK-Laminaten aus Gewebe-Prepreg, Prüfung in Kett- oder Schussrichtung, 1996.

[18] Stellbrink K K U. Micromechanics of composites. Composite properties of fibre and matrix constituents. Munich, Vienna, New York, 1996.

[19] Puck A. Festigkeitsanalyse von Faser-Matrix-Laminaten. München, Wien, 1996.

[20] VDI-Richtlinie. VDI 2014, Development of fibre-reinforced plastic composites. Analysis. Berlin, 2007.

[21] Puck A, Schürmann H. Failure analysis of FRP laminates by means of physically based phenomenological models. Special issue, Composites Science and Technology 1998; 58: 1045–1067.

[22] Puck A, Schürmann H. Failure analysis of FRP laminates by means of physically based phenomenological models. Special issue, Composites Science and Technology 2002; 62: 1633–1662.

[23] Schürmann H. Konstruieren mit Faser-Kunststoff-Verbunden. Berlin, Heidelberg, New York, 2005.

[24] Knops, M. Sukzessives Bruchgeschehen in Faserverbundlaminaten. D82, Dissertationsschrift, RWTH Aachen, Aachen, 2003.